Original article

Numerical study of buoyancy-driven natural ventilation in a simple three-storey atrium building

Shafqat Hussain, Patrick H. Oosthuizen [*]

Department of Mechanical and Materials Engineering, Queen's University, 130 Stuart, Kingston, ON K7L 3N6, Canada

Abstract

A simple three-storey atrium building was modeled to investigate the development of buoyancy-driven natural ventilation airflows induced by solar radiation and by the heat sources present on each floor of the building using a validated Computational Fluid Dynamics (CFD) model. The Reynolds Averaged Navier–Stokes (RANS) modeling approach with the SST-k-ω turbulence model and the Discrete Transfer Radiation Model (DTRM) was used for the numerical solution. The steady-state governing equations were solved using a commercial CFD solver FLUENT©. The air flow patterns, temperature distributions and the ventilation flow rates as predicted by the CFD model for this case study are presented in this paper. The ventilation flow rates were compared in non-dimensional form with the analytical design curves found in literature developed through the use of an analytical approach for a simple geometry atrium building. It was found that the CFD predictions agreed with the general trends described by the analytical model. The effect of solar intensity on the buoyancy-driven ventilation flow rates and the temperature distributions during the day-light hours and at different geographical locations was also investigated.

1. Introduction

Over recent decades natural ventilation has been widely recognized as one means of achieving low energy building design. Conventional ventilation systems based on mechanical components consume electric power. Due to the worldwide energy crisis, the need to reduce energy use in buildings has increased interest in natural ventilation strategies. Wind is the main cause of natural ventilation but in the absence of wind, the alternative is to implement stack pressure as the natural force to drive a ventilation flow. The difference between the external and internal pressures is the stack pressure available which can be created naturally by density differences to drive a ventilation flow through the building. Architectural features that can enhance the stack effect, for example, tall solar chimneys, light wells or atria are sometimes employed. These structures potentially increase the height of the column of warm air inside the buildings and, as a result, increase the stack driving force drawing cooler air from the exterior – near the bottom or sides of the building – and venting it out after it has warmed from convective heat exchange with the internal space of the building. Advanced stack-venti-

* Corresponding author. Tel.: +1 613 533 2573.
E-mail address: oosthuiz@me.queensu.ca (P.H. Oosthuizen).

lated atria buildings have the potential to consume less energy for space conditioning than typical mechanically ventilated buildings. The proper design of the natural ventilation system must be based on the detailed understanding of airflows within enclosed spaces governed by pressure differences due to wind and buoyancy forces. At the design stage, CFD modeling techniques can be utilized to investigate the ventilation flow rates, the temperature distribution and the thermal stratification within the ventilated space.

Simple building geometries such as a single ventilated enclosure with openings connected to the exterior have been the subject of much research in order to gain a deeper understanding of the ventilation concepts (Linden et al., 1990; Hunt and Kaye, 2001; Cook et al., 2003). The key concern when devising these sorts of ventilation strategies is whether sufficient ventilation will be generated. Presently CFD methods are being increasingly employed for predicting building airflows and testing natural ventilation strategies e.g., see (Anne et al., 2001; Atif and Claridge, 1995; Guohui, 2006; Josef et al., 2008; Kevin, 2007; Stavrakakis and Koukou, 2008; Tahir and Osman, 2005; Tsou, 2001; Oosthuizen and Lightstone, 2009). With the recent advances in computing power, the process of creating a CFD model and analyzing the results has become much less labor-intensive, reducing the time and therefore the cost. Compared to experimental and mathematical analysis, CFD techniques can provide more detailed information about velocity, turbulence and temperature distribution in the flow field. This information can be used easily for the thermal comfort analysis of the occupied areas of the buildings, e.g. see (Zhai, 2006; Jiang et al., 2004; Xin et al., 2009; Walsh and Leong, 2004; Stamou and Katsiris, 2006; Rundle et al., 2011; Josef et al., 2008). In addition, these techniques also allow the investigation of the effects of the geometrical design changes on the performance of the building to be performed easily.

Ji (2004, 2007) studied the flow characteristics (thermal stratification and airflow rates) of buoyancy-driven ventilation in an atrium connected to single storey space by using a CFD model. The numerical results were compared with predictions of analytical models and small-scale experiments. It was observed that the airflow patterns, temperature distribution and ventilation flow rates predicted by the CFD model agreed favorably with the analytical models and the experiments. Cook and Lomas (1998) showed comparisons between analytical, experimental and CFD modeling of natural convection airflow in a single space with a localized point heat source and openings connected to the ambient environment. Allocca et al. (2003) investigated the effect of single sided natural ventilation for a stack of rooms sharing a vertical ventilation space. A CFD model was used to assess the effects of buoyancy and wind on the ventilation flow rates and the indoor conditions. Predicted results were compared with empirical and analytical solutions for the buoyancy-driven flow. The researchers considered heat sources from the rooms and noted that the CFD results were within 10% of analytical solutions for buoyancy driven flow.

Holford and Hunt, (2003) studied the flow field in a single ventilated space connected to a tall atrium and developed simple analytical models which they validated using small-scale salt bath experiments. It was shown that at the design stage these techniques can be useful for understanding the flow characteristics, including the likely ventilation flow rate, fresh air distribution and temperature distributions. To observe the applicability of the analytical techniques suggested by Holford and Hunt, (2003), a simple three-storey atrium building was designed in the present work to investigate the use of buoyancy-driven natural ventilation. The theoretical features of these techniques are described here briefly:

The buoyancy-driven ventilation flow rate in a heated atrium building may be enhanced by increasing the depth or temperature of the warm air that collects in the upper region of the space. By considering a space with two small ventilation openings separated by a vertical height, Δd, (Fig. 1), a layer of cool ambient air of temperature T_0, and density ρ_0, underlies a warmer layer of temperature $T = T_0 + \Delta T > T_0$ and density $\rho = \rho_0 - \Delta \rho < \rho_0$, that extends down a depth $= H - h$ below the upper opening. The hydrostatic pressure between the openings is:

$$\Delta p_{\text{external}} = \rho_0 g \Delta d \ (\textit{outside the building})$$

$$\Delta p_{\text{internal}} = \rho_0 g \Delta d - \Delta \rho g h \ (\textit{inside the building})$$

The difference between the external and internal pressures is the stack pressure available to drive a flow through the space. In other words, the pressure difference associated with the depth of the warm layer between the openings drives the flow. Fig. 1 shows an enclosure connected to an atrium. The shading represents the warm air in the upper regions of the room and atrium (Holford and Hunt, 2003).

The volume flow rate Q of unidirectional flow through an opening of area, a, depends on the driving pressure drop Δp across it and is given by:
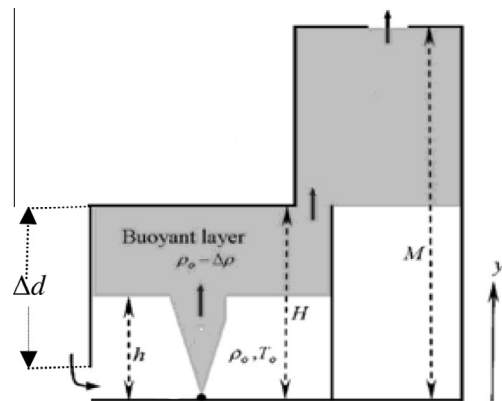
Fig. 1. Enclosure connected to an atrium. The shading represents the warm air in the upper regions of the room and atrium (Holford and Hunt, 2003).

$$Q = \sqrt{2} c_{d^a} \sqrt{\frac{\Delta P}{\rho_0}} \tag{1}$$

where c_d is the discharge coefficient and is determined empirically. The discharge coefficient is generally combined with the opening area to define the effective area,

$$A^* = \sqrt{2} c_{d^a} \tag{2}$$

Morton et al. (1956) performed theoretical analysis of the turbulent plume of buoyant fluid above a point source, of strength B, and noted that if the plume has no initial momentum and volume flux, then the volume flux Q at a height h above the source is related by:

$$Q(h) = c(Bh^5)^{1/3} \tag{3}$$

where $c \approx 0.14$ and is a constant related to the entrainment coefficient α for a plume and B is the buoyancy flux. In the steady state, the volume flux driven through the openings by the stack pressure must equal the volume flux in the plume at the interface. Hence, the interface height (h_{storey}) satisfies the equation:

$$\left(\frac{h_{storey}}{H}\right)^5 = \left(\frac{A^*_{storey}}{H^2}\right)^2 \left[1 - \left(\frac{h_{storey}}{H}\right)\right] \tag{4}$$

where H is the storey height and A^*_{storey} is the effective area of the storey openings, related to the lower and upper storey opening effective areas by the relation:

$$\frac{1}{A^{*2}_{storey}} = \frac{1}{A^{*2}_{storey-lower\ opening}} + \frac{1}{A^{*2}_{storey-upper\ opening}} \tag{5}$$

When the flow is steady, the flow rate in the plume in the storey at the interface height (h_{storey}) equals the flow rate through the storey which is given by:

$$Q_{storey} = ch^{5/3} \tag{6}$$

where $c \sim 0.14$ and is a constant related to the entrainment coefficient for a plume. Ventilation flow rates and interface heights were non-dimensionalized based on the storey parameters, choosing H as the length scale and $(H/B)^{1/3}$ as the timescale where B is the buoyancy flux. Non-dimensional interface height is defined as $\frac{h}{H}$, where H is storey height.

Non-dimensional volume flow rate is defined as:

$$\frac{Q_{storey}}{cB^{1/3}H^{5/3}} = \left(\frac{h_j}{H_j}\right)^{5/3} \tag{7}$$

Non-dimensional total effective area of the flow path is defined as $\frac{A_t}{H^2}$ where the total effective area of the flow path (A_t) is defined as

$$\frac{1}{A_t^2} = \frac{1}{A^2_{storey}} + \frac{1}{A^2_{exhaust}} \tag{8}$$

A ventilation strategy in which the same total effective opening area is used for each floor in a multi-storey building, an equation set, was derived by Holford and Hunt (2003) in the following form:

$$C^3 \left(\left(\frac{1}{A_{0s}^2}\right)h_0^{\frac{10}{3}} + \left(\frac{1}{A_{exhaust}^2}\right)\left(h_0^{\frac{5}{3}} + h_1^{\frac{5}{3}} + h_2^{\frac{5}{3}}\right)^2\right)$$
$$= h_0^{-\frac{5}{3}}(H - h_0) + \frac{3(M - H)}{h_0^{\frac{5}{3}} + h_1^{\frac{5}{3}} + h_2^{\frac{5}{3}} +} \tag{9a}$$

$$C^3 \left(\left(\frac{1}{A_{1s}^2}\right)h_1^{10/3} + \left(\frac{1}{A_{exhaust}^2}\right)\left(h_0^{5/3} + h_1^{5/3} + h_2^{5/3}\right)^2\right)$$
$$= h_1^{-5/3}(H - h_1) + \frac{3(M - 2H)}{h_0^{5/3} + h_1^{5/3} + h_2^{5/3}} \tag{9b}$$

$$C^3 \left(\left(\frac{1}{A_{2s}^2}\right)h_2^{10/3} + \left(\frac{1}{A_{exhaust}^2}\right)\left(h_0^{5/3} + h_1^{5/3} + h_2^{5/3}\right)^2\right)$$
$$= h_2^{-5/3}(H - h_2) + \frac{3(M - 3H)}{h_0^{-5/3} + h_1^{-5/3} + h_2^{-5/3}} \tag{9c}$$

where subscripts 0, 1, and 2 represent first, second and third, storey respectively.

For a ventilation strategy to achieve the same ventilation flow rate for each storey, the equation was derived as

$$\frac{A_{jt}}{H^2} = \left(\frac{c^3(h/H)^5}{\frac{(M-jH)}{H} - \left(\frac{h}{H}\right)_j + \frac{B_{solar}}{B}\left(\frac{M}{H} - 1\right)}\right)^{1/2} \tag{10}$$

Using these equations, Holford and Hunt (Holford and Hunt, 2003) developed design curves which were validated against the salt bath experimental measurements for sizing the ventilation openings in a multi-storey building connected to an atrium. These equations indicate that the interface height separating the buoyant upper layer at temperature T_j, and the lower layer at ambient temperature T_0, depends on geometric factors such as the storey height, H_j, the atrium height, M, the effective areas of the storey, the atrium outlet and the constant, c.

The purpose of the present study was to numerically investigate the development of the buoyancy-driven natural ventilation airflow and temperature distributions induced by solar radiation and heat sources present on each floor of a simple atrium building by utilizing the validated and tested CFD model. The CFD model was also evaluated by comparing the numerical results obtained against the design curves developed by Holford and Hunt (2003) who considered more general cases for these types of buoyancy-driven natural ventilation airflows.

2. Building description

The thermal environment in the atrium space of the Engineering Building of Concordia University, Montreal was previously studied by the authors using a CFD model and the CFD predictions were validated against the experimental data available e.g., see Refs. (Hussain and Oosthuizen, 2010, 2011a,b, 2012a; Hussain et al., 2011). Based on the analysis of these previous studies (Hussain and Oosthuizen, 2010, 2011a,b, 2012a; Hussain et al., 2011) and keeping in mind the possible use of the design curves developed

by Holford and Hunt (2003) for a simple atrium building, a full-scale simple atrium building was modeled. The selected geometry of the simple atrium building is shown in Fig. 2. The significant dimensions and areas of the building are given in Table 1. The values of the climatic parameters used in the CFD simulations are shown in Table 2. In order to utilize the validated CFD model (Hussain and Oosthuizen, 2010, 2011a,b, 2012a; Hussain et al., 2011), the simulated building was assumed to have the same location and orientation as the Engineering building at Concordia University, Montreal, Canada, i.e., 35 degrees west of south, with the same kind of façade glazing surface facing southwest. The atrium exhausts were located on the highest point in the atrium and storey inlets and outlets on each storey were located on the side walls of the rooms (Fig. 1). The inlets and outlets were sized on each storey using the design curves developed by Holford and Hunt (2003). The effective atrium outlet opening area was selected to be equal to the total inlet opening areas for each storey.

3. Numerical solution procedures

3.1. CFD model

The airflow patterns and temperature distributions in the atrium building are governed by the conservation laws of mass, momentum and energy. The mathematical model applied includes the numerical techniques to solve the continuity, Navier–Stokes (N–S), and energy equations for incompressible, three-dimensional and turbulent flow. The general form of the momentum, turbulent kinetic energy, turbulent energy dissipation, and energy (temperature for constant heat capacity) equations in the steady-state form can be expressed in the general form as follows:

Fig. 2. The simple three-storey atrium building.

Table 1
Dimensions and areas of the atrium building.

Dimensions and areas	
Atrium height	16.00 m
Atrium width	5.00 m
Atrium depth	6.00 m
Room height	4.00 m
Room width	6.00 m
Room depth	6.00 m
Façade glazing area	80.00 m^2
Ground floor air supply (net) area	0.80 m^2
First floor air supply (net) area	1.00 m^2
Second floor air supply (net) area	1.60 m^2
Atrium outlet opening (net) area	3.40 m^2

$$\frac{\partial(\rho u_i \phi)}{\partial x_i} = \frac{\partial}{\partial x_i}\left(\Gamma_\phi \frac{\partial \phi}{\partial x_i}\right) + S_\phi \tag{11}$$

where variable (ϕ) is $(\phi) = (u), (v), (w), (k), (\varepsilon), (h, T)$, respectively, Γ_ϕ is the diffusion coefficient of the variable (ϕ) and S_φ represents the source terms including the pressure terms, thermal source terms, etc., as appropriate for the variable (ϕ) being solved. It has been assumed that: (a) single phase, steady-state flow for a Newtonian fluid exits, (b) heat transfer at the walls by either conduction or radiation is neglected, except at the glazing walls (c) steady-state atmospheric conditions exist, (d) wind velocity is zero. A CFD model of a simple three-storied atrium building (see Fig. 2) was prepared using the commercial CFD software FLUENT©. For this model the key dimensions are the atrium height ($M = 16$ m) and the storey height ($H = 4$ m). Based on the atrium height, a Rayleigh number for the system that is greater than 1.0×10^9 indicates the onset of turbulence in the flow field. Consequently a turbulence model was employed in the CFD simulations. When the first-order fluid parameters are of main concern (e.g., mean temperature and flow rate) rather than turbulent fluctuation details, generally two equation eddy-viscosity turbulence models are thought suitable for modeling indoor flows. It was noted from previous studies (Hussain and Oosthuizen, 2010, 2011b, 2012a,b; Hussain et al., 2011) that the SST k-ω turbulence model with the DTRM radiation model is suitable for the present CFD simulations.

The numerical procedures followed in these previous studies were utilized in the present CFD simulations. The pressure coupling was treated using the SIMPLE algorithm. The body force weighted scheme was used to discretize pressure–velocity coupling. The second-order upwind scheme was used to discretize the momentum, turbulent kinetic energy, dissipation rate and energy conservation equations. These were solved in a segregated manner. The convergence of the solution was considered to have been reached when the enthalpy residual was less than 0.1% and the flow variables having low values of residuals, say 10^{-3}. The under relaxation factors for pressure, density, momentum, turbulence kinetic energy, turbulence dissipation rate, turbulent viscosity, and energy (0.3, 1.0, 0.2,
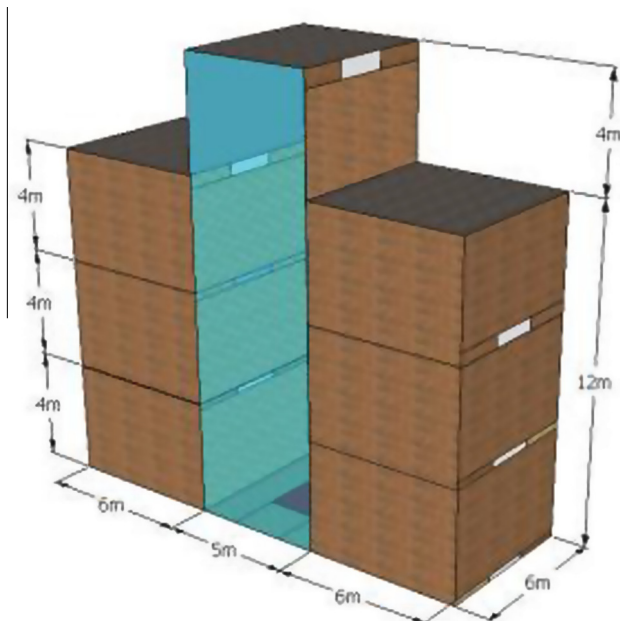
Table 2
Solar irradiation and outside conditions in Montreal at 13:00 h on July 15, 2010.

Sun direction vector	x	y	z
	-0.54	0.84	-0.06
Sunshine fraction	1 (full shine)		
Direct normal solar irradiation (at Earth's surface) [W/m²]	863		
Diffuse solar irradiation – vertical surface (W/m²)	137		
Diffuse solar irradiation – horizontal surface (W/m²)	109		
Ground reflected solar irradiation-vertical surface (W/m²)	88		
Outside heat transfer coefficient (W/m²-°C)	7.4		
Outside air temperature (°C)	25		

0.8, 0.8, 1.0, 0.9, respectively) were used to arrive at the converged solution. Simulations were performed on a desktop PC with Intel Quad Core Processor (EM 64 T Family 6 Model 15 Stepping 11 Genuine Intel ~3.0 GHz), 8 GB Ram 1333 Hz, Windows XP Professional 64 bit SP2 Operating system and required approximately 24 h to complete for the grid selected.

3.2. Radiation model

Heat transfer by thermal radiation is an extremely important consideration in many modeling cases such as the case being investigated here. To account for radiation, radiation intensity transport equations (RTEs) are solved. Local absorption by fluid and at boundaries links RTEs with energy equation. The solar radiation was considered to transmit through the glazing façade wall and heat up interior surfaces of the building, as well as partially absorbed at the glazing façade wall. The solar calculator was used to determine the sun's location with the given

inputs of time, date and the global location. Solar irradiation and outside conditions calculated at 13:00 on July 15, 2010 are shown in Table 2. A solar calculator is also available in FLUENT© to calculate the beam direction and irradiation. The DTRM radiation model was found suitable to model the radiation for the present study. The main assumption followed in the DTRM model is that radiation leaving a surface element in a specific range of solid angles can be approximated by a single ray. It uses a ray-tracing algorithm to integrate radiant intensity along each ray and is a relatively simple model. Accuracy can be increased by increasing the number of rays to a wide range of optical thicknesses.

3.3. Boundary conditions

External climatic conditions affect the architectural design of naturally ventilated buildings. The internal air-flow pattern is the result of interaction between the indoor and outdoor environment. In particular, natural ventilation, and outdoor conditions strongly affect the indoor air-flow pattern, and thus affect the thermal sensation of the occupants. In the present study the focus was to investigate the use of buoyancy-driven natural ventilation during day time, therefore numerical investigations were performed under fixed steady state outdoor climatic conditions with an ambient temperature of 25 °C at 13:00 h on July 15, 2010 which represents the weather data for the location of the reference building while wind velocity was assumed to be zero. The natural ventilation of the building was considered based on only buoyancy-driven natural ventilation induced by the heat gains from the solar radiation and other heat sources present in the building. For turbulence the specification method (intensity and hydraulic diameter) was used and turbulence intensity (%) = 0.05 was applied
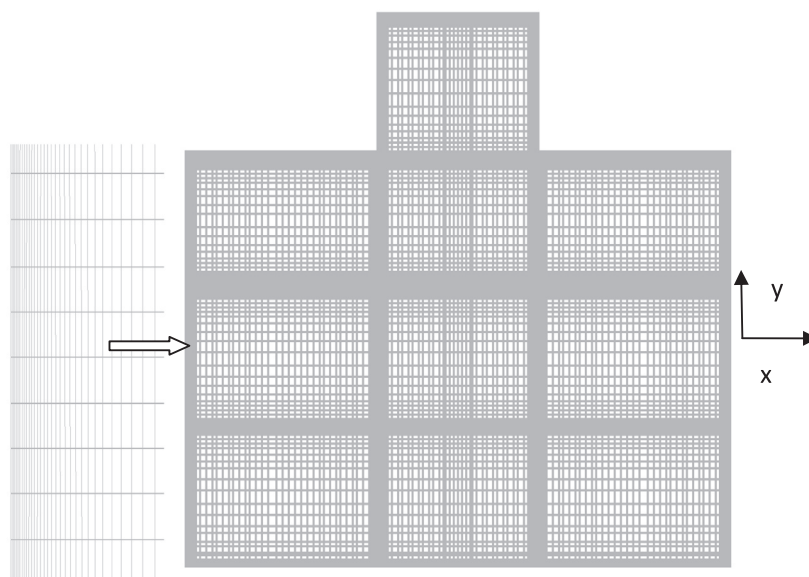
Fig. 3. Mesh structure for CFD simulations (Mesh 2) with an expanded view being shown on the left.

Table 3
Volume flow rates at three floors using three mesh densities.

Floors	Volume flow rate (m³/s)		
	Mesh 1	Mesh 2	Mesh 3
Ground floor	0.42	0.42	0.42
First floor	0.42	0.42	0.42
Second floor	0.40	0.40	0.40

at the inlets as the boundary conditions. The heat sources were assumed to be located in the center of each floor to match with the assumptions of the mathematical models developed by Holford and Hunt (2003).

In practice, airflow inside the connected spaces is mixed by conduction, convection and radiation heat transfer effects. In this work, conduction and radiation effects were only considered for the glazed façade wall while all the other walls were assumed to be adiabatic to meet the assumptions of the mathematical models developed by Holford and Hunt (2003). All boundaries of the domain, except the glazed façade surface, ventilation openings, and heat sources were modeled as no-slip ($u_j = 0$) wall boundaries with zero heat flux. The mixed thermal boundary conditions were used for the glazed façade surface. One of the most demanding aspects of heat transfer through the glazed façade surface is the evaluation of the convection heat transfer coefficient. There are many different correlations in the literature to determine the external heat transfer coefficient for the buildings. Palyvos (2008) summarized different correlations found in the literature. On the basis of thirty available linear correlations, Palyvos recommended using the following correlation (Eq. (12)) to calculate the heat transfer coefficient (h_c) for windward surfaces:

$$h_c = 4V_w + 7.4 \tag{12}$$

where V_w is wind velocity. With zero wind velocity, an external heat transfer coefficient value of 7.4 W/m²-K was

used. The optical properties of the glazed façade surface (semi transparent), i.e., a solar transmittance of 36% and an absorptivity of 17.5%, were the same as those used in previous studies (Hussain and Oosthuizen, 2010, 2011a,b, 2012a; Hussain et al., 2011) of an existing atrium building at Concordia University. The modeling of the glazed façade was simplified as a single glazed wall with an effective thermal conductivity of 0.0626 W/m²-K and a total overall thickness of 24 mm. The radiation exchange between the façade and the sky was also taken into account. The sky temperature was calculated using the (Mills, 1999) correlation, $T_{sky} = [\varepsilon_{sky} T_{out4}]^{1/4}$ where the emissivity of the sky, ε_{sky}, was calculated using the relation, $\varepsilon_{sky} = 0.727 + 0.0060\ T_{out}$ with an ambient temperature of T_{out}, of 25 °C. The heat sources were modeled as a no-slip wall boundary (2×2 m) located in the center of each floor. In all cases the buoyancy flux value, B, was assumed to be 22.63×10^3 m⁴ s³ (a heat source of 823 W was assumed approximately equivalent to four sitting persons with desktop computers) on each room floor and 14.57×10^3 m⁴ s³ (a heat source of 530 W was assumed approximately equivalent to seven resting persons) on the atrium floor. A constant relative pressure of 0 Pa was used across the room inlets and the atrium outlet.

3.4. Mesh dependency test

The hexahedral cells were created with fine mesh near the walls of the simple three-storey atrium building (Fig. 2) using the commercial software GAMBIT©. The grid along the vertical plane parallel to the façade glazing surface is shown in Fig. 3. Three mesh densities were investigated: Mesh 1 (415,000 cells), Mesh 2 (812,000 cells, see Fig. 3) and Mesh 3 (1,235,000 cells). In all meshes, more cells were located where higher velocity and temperature gradients were expected i.e., near walls, ventilation open-
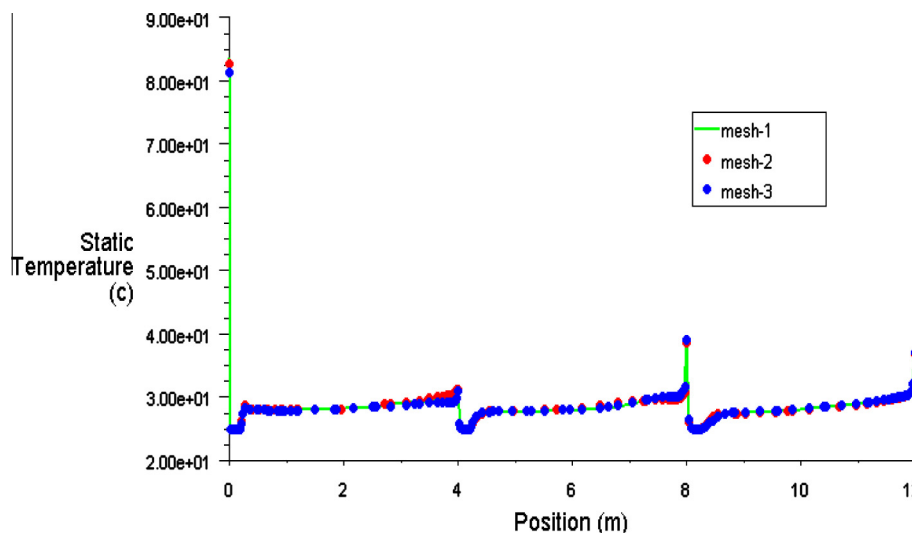
Fig. 4. Prediction of vertical temperature profile in the center of rooms for different mesh densities, where 0, 4 and 8 m define the ground, first and second floor levels respectively.

Table 4

Comparison of the numerical predictions and experimental measurements of indoor air temperatures using SST k-ω turbulence model.

Y (m)	Temperature T (°C)								
	$x = 5.96$, $z = 7$ m			$x = 5.78$, $z = 1.05$ m			$x = 8.81$, $z = 4.447$ m		
	Measured	Predicted	% error	Measured	Predicted	% error	Measured	Predicted	% error
2.1	24	22.87	4.7	22.3	22.37	0.3	23	22.71	0.5
6.16	24.5	24.55	0.2	25.1	24.47	2.5	24.6	24.72	0.4
10.25	26.2	26.52	1.1	26.1	26.20	0.4	26.3	26.55	0.3

Table 5

Variation in the volume flow rate of the buoyancy-driven ventilation in the left-hand side rooms of the building with the increase of inlet opening area in each storey.

Inlet opening area on each floor (m²)	Total effective opening area (A_t/H^2)	Volume flow rate (m³/s)			Air changes per hour (ACH)		
		Left-hand side rooms			Left-hand side rooms		
		Ground floor	First floor	Second floor	Ground floor	First floor	Second floor
0.2	0.0087	0.27	0.22	0.17	7	5	4
0.4	0.017	0.44	0.34	0.25	11	8	6
0.6	0.026	0.59	0.42	0.32	15	11	8
0.8	0.035	0.75	0.65	0.45	19	16	11
1	0.044	0.85	0.66	0.45	21	16	11

ings and the area potentially occupied by the thermal plume in order to capture the details of the airflow in these areas. The numerical results indicating the volume flow rates in the left-hand side rooms of the building using three mesh densities are given in Table 3. Vertical temperature profile in the center of left-hand side rooms for different mesh densities is shown in Fig. 4 where 0 m, 4 m and 8 m define the ground, first and second floor levels respectively. It can be seen that there is a very small difference between the results obtained using the three meshes indicating that the results are essentially mesh independent. Considering both accuracy and computational time, it was decided that Mesh 2 (812,000 cells) was suitable to accurately predict volume flow rate, airflow and temperature distributions in the building. Approximately 10,000 iterations were required for the cases considered here to meet the convergence criteria.

4. Results

The proposed general ventilation concept involves fresh air being taken in from openings in the east and west facing walls, passing through the occupant space, and flowing out from upper openings between the rooms and the atrium. The air is finally exhausted from the atrium outlet at the top of the building. It is assumed that the driving force is the difference between the inside and outside temperatures of the building without considering the affects of external wind. Buoyancy-driven natural ventilation is more complex and difficult to model because several parameters that are involved are dependant and interdependent on the driving force of the ventilation. To cover all of these parameters is

beyond the scope of the present paper. Here, factors such as climate conditions, radiation intensity and various geographical locations were considered and will be discussed in detail to elucidate the performance of buoyancy-driven ventilation in the prototype residential building. Other parameters will be investigated in future studies.

4.1. Validation of the CFD model

The CFD model used in this work was validated in recent studies i.e., see (Hussain and Oosthuizen, 2010, 2011a,b, 2012a; Hussain et al., 2011) for the prediction of the airflow and temperature distributions in the atrium space of an Engineering building of Concordia University, Montreal, and an atrium building in Ottawa, Canada. The validation was carried out by comparing the CFD predictions against the experimental measurements. A close agreement was found between the CFD predictions and experimental measurements which demonstrates the ability of the CFD model used to accurately predict three-dimensional buoyancy-driven displacement ventilation flows in multi-storey spaces connected to a common atrium. For the Concordia building, the average air temperatures along the height of the atrium were predicted at 16:00 h on August 1, 2007 and compared with the experimental data obtained by Mouriki (2009). For example, a comparison of the air temperatures predicted by the numerical model used and the measured temperature values at different locations in the atrium space of the Engineering building at Concordia University Montreal, Canada is shown in Table 4. The difference between the predictions and mea-
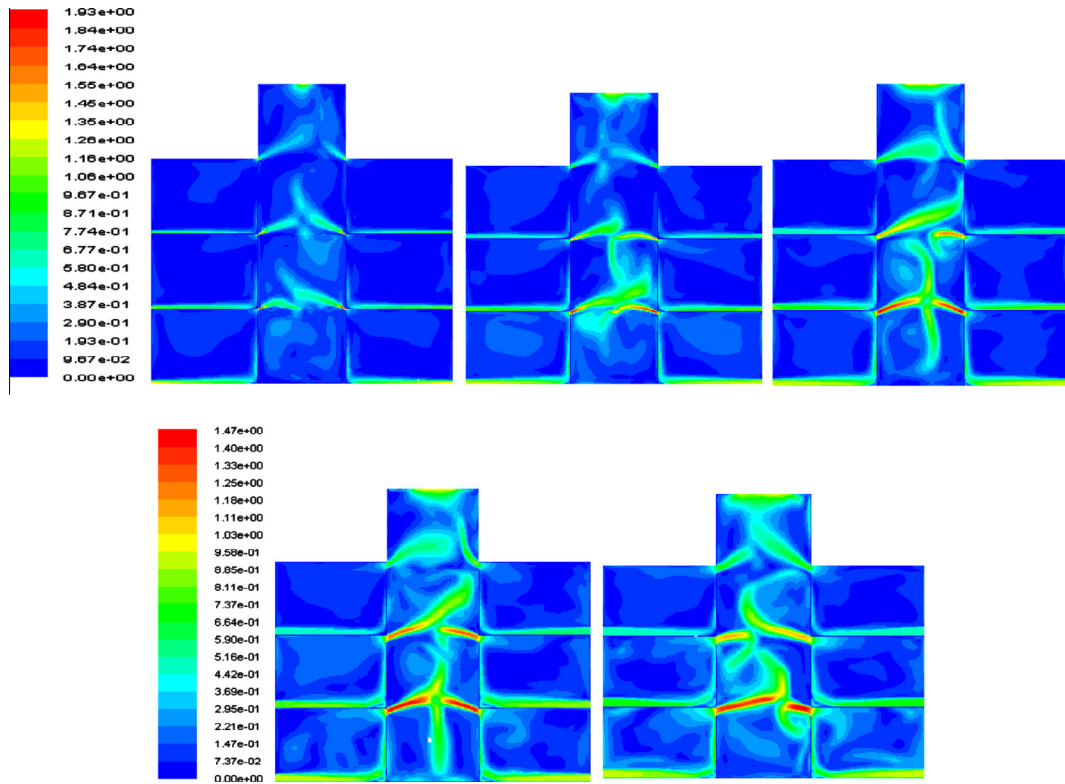
Fig. 5. CFD predictions of the effect of increasing the inlet opening area (given in Table 5) on velocity (m/s) contours with the same inlet opening area for each storey.
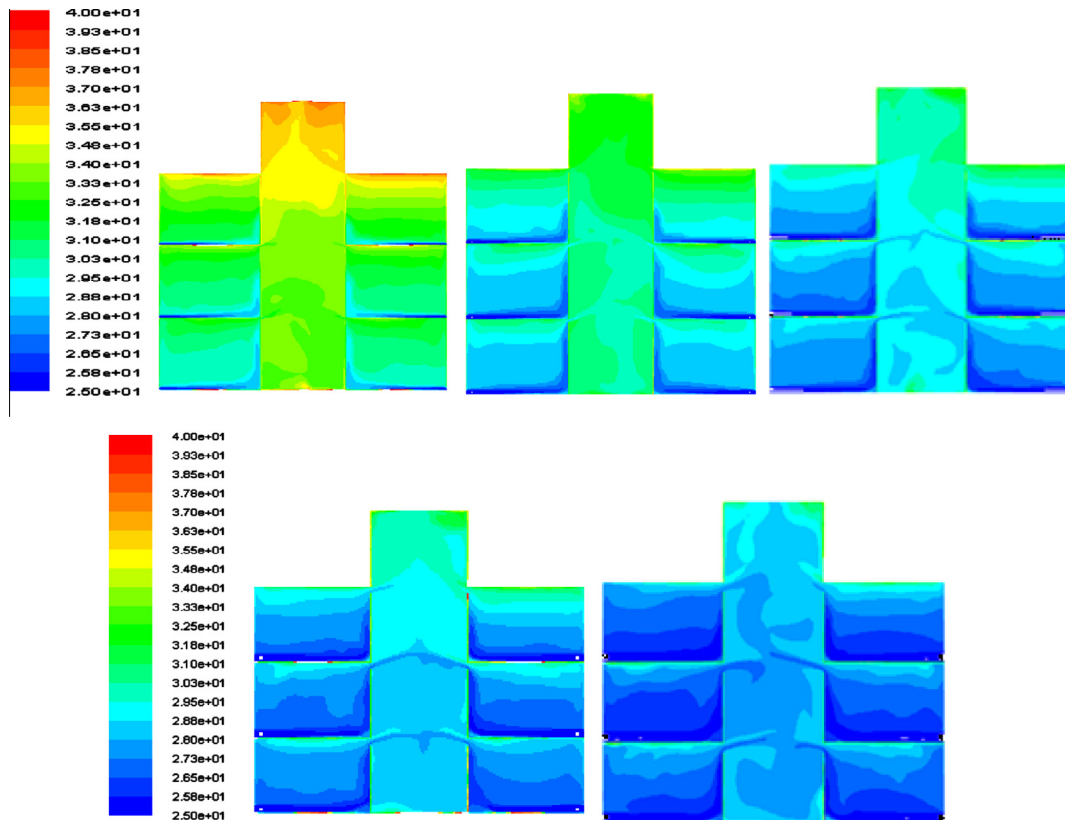
Fig. 6. CFD predictions of the effect of increasing the inlet opening area (given in Table 5) on temperature (°C) contours with the same inlet opening area for each storey.
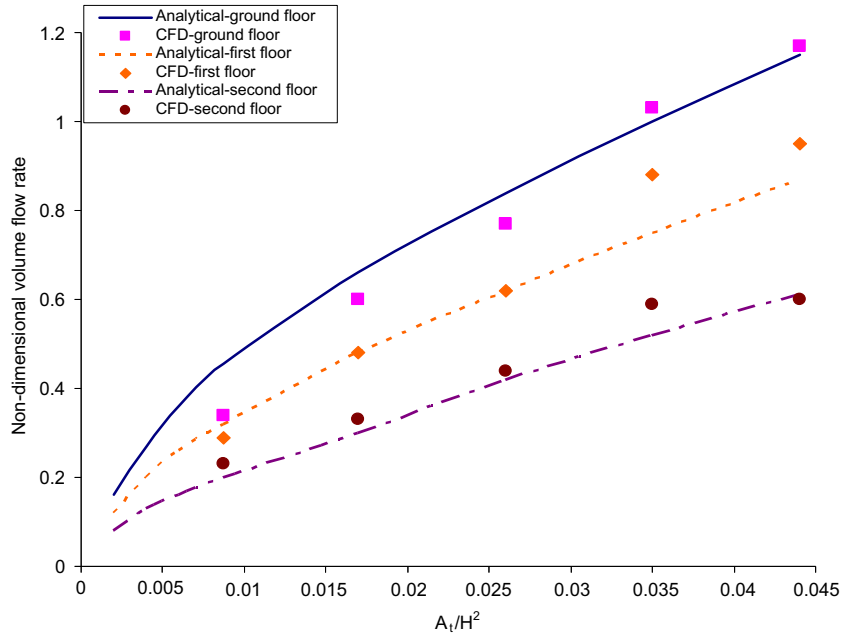
Fig. 7. Comparison between the CFD model predictions and the analytical model predictions (Holford and Hunt, 2003) for the volume flow rate for the situation where the same total effective opening area (A_t/H^2) is used for each storey of the building.

Table 6
Volume flow rates (m³/s) and air changes per hour (ACH) with different inlet opening areas on each floor of the building.

Floors	Inlet opening area (m²)	Total effective opening area (A_t/H^2)	Volume flow rate (m³/s)		Air changes per hour (ACH)	
			Left side	Right side	Left side	Right side
Ground floor	0.40	0.0170	0.42	0.42	12	12
First floor	0.50	0.0235	0.42	0.42	12	12
Second floor	0.80	0.0380	0.40	0.41	11	12
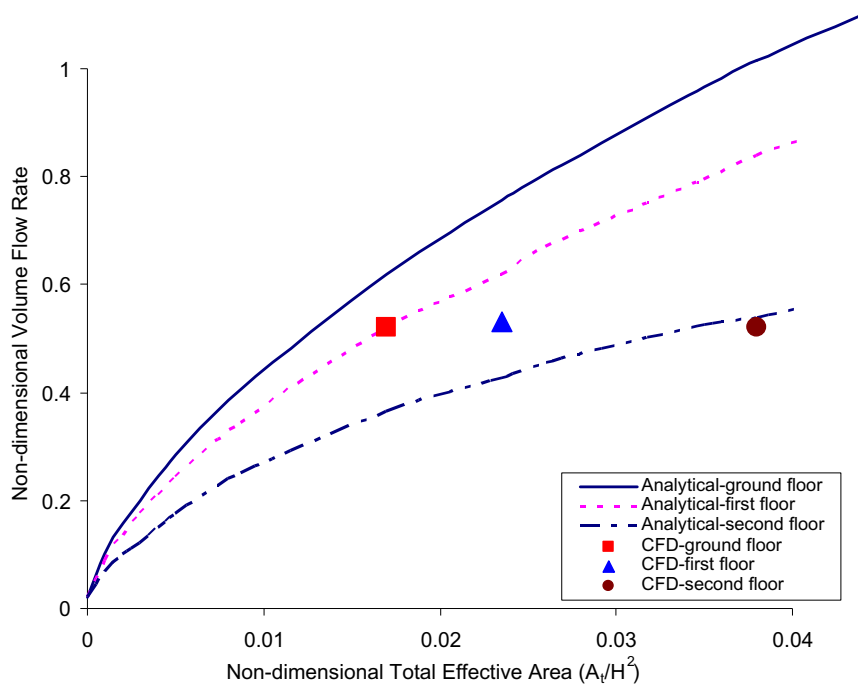
Fig. 8. Comparison of the analytical results and the CFD predictions for the non-dimensional volume flow rate where the openings were sized to give the same ventilation flow rate on each storey.

Table 7a
Buoyancy-driven volume airflow rate with variation in internal heating load in the left-hand side rooms and atrium space of the building located in Montreal at 13:00 h on July 15, 2010.

Left-hand side rooms	Volume flow rate (m^3/s) (100 W/m^2)	Volume flow rate (m^3/s) (200 W/m^2)	Volume flow rate (m^3/s) (300 W/m^2)	Volume flow rate (m^3/s) (400 W/m^2)	Volume flow rate (m^3/s) (500 W/m^2)
Ground floor	0.39	0.42	0.45	0.47	0.49
First floor	0.39	0.42	0.45	0.47	0.49
Second floor	0.37	0.41	0.44	0.46	0.48

Table 7b
Buoyancy-driven volume airflow rate with variation in internal heating load in the right-hand side rooms of the building located in Montreal at 13:00 h on July 15, 2010.

Right-hand side rooms	Volume flow rate (m^3/s) (100 W/m^2)	Volume flow rate (m^3/s) (200 W/m^2)	Volume flow rate (m^3/s) (300 W/m^2)	Volume flow rate (m^3/s) (400 W/m^2)	Volume flow rate (m^3/s) (500 W/m^2)
Ground floor	0.39	0.42	0.45	0.47	0.49
First floor	0.39	0.42	0.45	0.47	0.49
Second floor	0.37	0.41	0.44	0.46	0.48

surements has been expressed in terms of percentage error (%), see Hussain and Oosthuizen (2012a).

A series of CFD simulations was run to investigate the various flow situations of buoyancy-driven ventilation in the building considered here. The numerical results obtained from the CFD simulations are presented in four sections: Section 4.2 presents the results for the simulations where the total effective opening area, A_{jt}, is the same for each storey. In Section 4.3 the results for the simulations where effective opening areas were sized to have the same ventilation flow rate in each storey are presented. Section 4.4 presents the results for the variation in the internal heat sources of the building. Section 4.5 describes the results of the effect of solar intensity on the ventilation volume flow rate and in Section 4.6 the effect of the geographical location of the building on the ventilation volume flow rate is presented.

4.2. CFD simulations using the same inlet opening area in each storey

The variation in volume flow rate expressed both in (m^3/s) and in air changes per hour (ACH) of the buoyancy-driven ventilation in each room (on the left-hand side of the building) with changes in the inlet opening area are given in Table 5. The CFD results indicating the velocity and temperature contours in the building with the same inlet opening area in each storey and the effect of the variation of the inlet opening area on the velocity and temperature contours are shown in Figs. 5 and 6 respectively.

It will be seen from Table 5 that with an increase in the inlet opening area on each floor the ventilation flow rate increases until it reaches a maximum. The CFD predictions of the volume flow rate in the non-dimensional form using Eq. (7) were compared with the analytical predictions obtained using design curves developed by Holford and Hunt (2003) for a simple geometry when the same effective

opening area (A_t/H^2) is used for each storey, the comparison being shown in Fig. 7. From the results it can be seen that the CFD predictions of the volume flow rates expressed in non-dimensional form agree fairly well with the general trends depicted by the design curves developed analytically by Holford and Hunt (2003). However, some discrepancies were observed, this is thought to be due to the assumption in the analytical model that the buoyant layer remains homogenous and hydrostatic for all interface heights which was not the case in the CFD simulations as the interface approached the ceiling. It is seen that the lower storey has higher volume air flow rate than the upper storey, while the temperature of the stratified layer in the upper storey is higher than that in the lower storey. From the numerical results obtained, it was noted that increasing the total effective opening area for each storey resulted in an increase in the volume flow rate. The same observation has been reported in the literature (Holford and Hunt, 2003). However, in order to obtain the same ventilation flow rate in each storey, the total effective opening area for each storey needs to be different. The higher storey requires a larger total effective opening area than the lower storey in order to compensate for the lower stack effect.

4.3. Openings sized to have same ventilation flow rate in each storey

The inlets in each storey are located on the side walls of the rooms (Fig. 2). They were sized for each storey using the design curves developed by Holford and Hunt (2003) to have approximately the same ventilation flow rate in each storey. Table 6 shows the results of volume flow rates (m^3/s) and air changes per hour (ACH) of the buoyancy-driven ventilation with these different total effective opening areas in each storey of the building and it was noted that in each storey the ventilation flow rates are almost equal. The CFD predictions of the volume flow rate
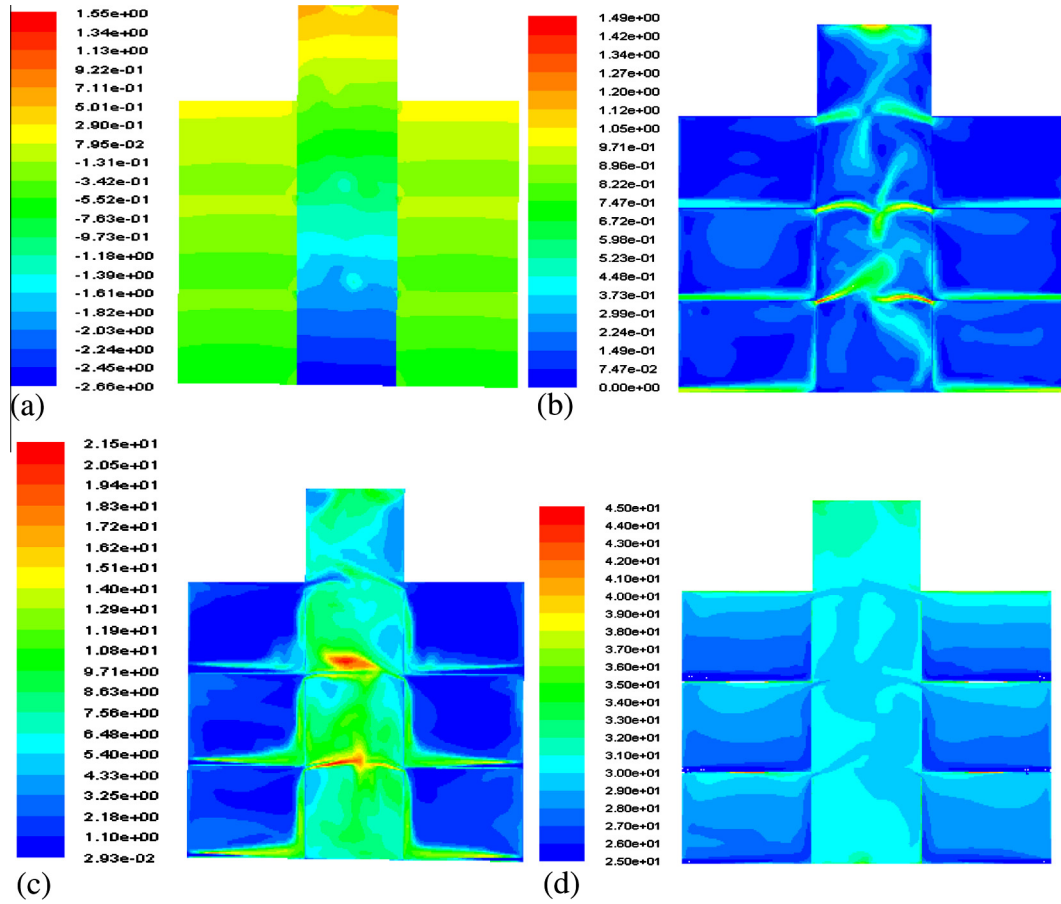
Fig. 9. Pressure (Pascal) (a), velocity (m/s) (b), turbulence intensity (%) (c) and temperature (°C) (d) contours in the middle plane parallel to the facade surface along the height of the building.
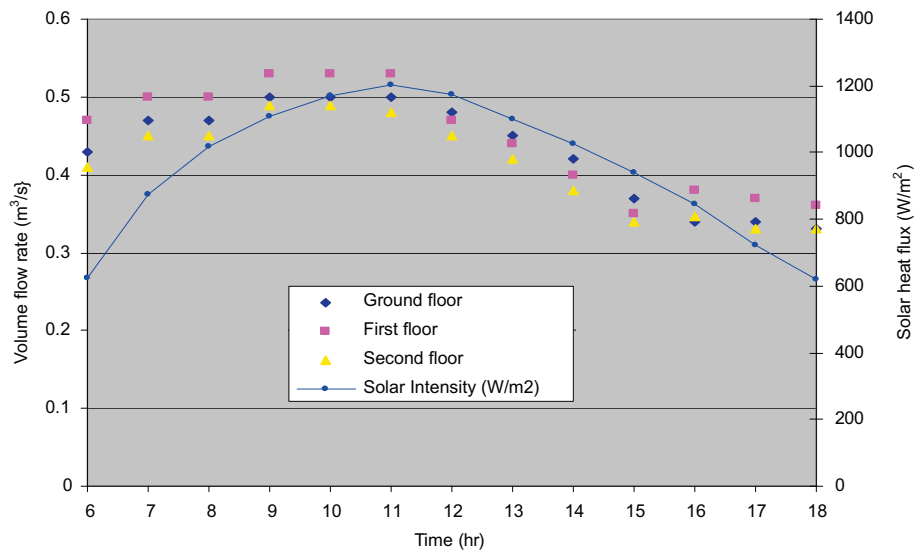
Fig. 10. Effect of solar intensity on the volume flow rate with the same ventilation rate in each storey.

expressed in the non-dimensional form were compared with the analytical predictions obtained using the design curves developed by Holford and Hunt (2003) and are shown in Fig. 8. From the results it was found that the

CFD predictions of the volume flow rates expressed in non-dimensional form agree well with the analytical design curves on second floor but are under predicted on the first and ground floors. This discrepancy can be attributed to

Table 8
Global position and ambient temperatures of each location at different dates.

Name of location	Global position		Outside temperature (°C)		
	Latitude	Longitude	April 15, 2010 (13:00 h)	July 15, 2010 (13:00 h)	September 15, 2010 (13:00 h)
Calgary (Alberta)	51	114	12	23.8	12.9
Winnipeg (Manitoba)	50	90	9.9	22.3	16.1
Montreal (Quebec)	45	73	10.7	29.7	14.4
St. John's (Newfoundland)	47	52	0	19.6	15.4
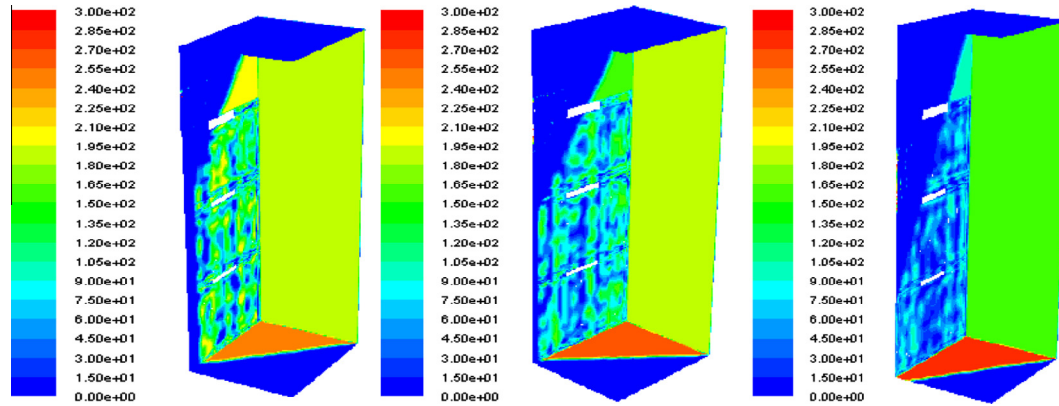
Fig. 11a. Contours of solar heat flux (W/m^2) on the façade, east wall and floor of the atrium at 13:00 h in Calgary (Longitude: −114, Latitude: 51) on April, July and September 15, 2010 respectively.
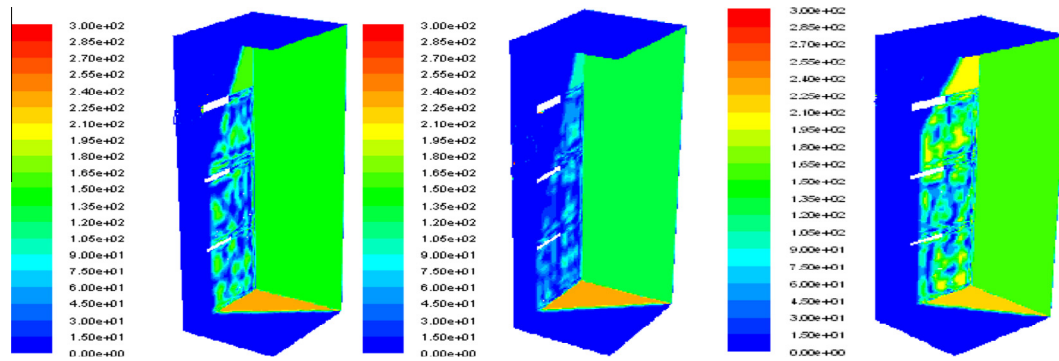
Fig. 11b. Contours of solar heat flux (W/m^2) on the façade, east wall and floor of the atrium at 13:00 h in Winnipeg (Longitude: −90, Latitude: 50) on April, July and September 15, 2010 respectively.

the fact that buoyancy effects (strong convection) are higher on the ground and first floors as compared to the second floor which becomes difficult to predict analytically. However, the analytical design curves developed by Holford and Hunt (2003) are helpful in selecting the sizes of inlet openings to have approximately same ventilation flow rates on each storey.

4.4. Indoor thermal load conditions

Here the volume airflow rates in the rooms and atrium space are evaluated using different heat-loading conditions. In this part of the simulations, an ambient temperature of 25 °C at 13:00 h on July 15th, 2010 in Montreal is used. Heat sources of 100, 200, 300, 400 and 500 W/m^2 were assumed which cover an area of 2×2 m in the center of each floor of the building considered. All other walls except the façade glazing wall were assumed adiabatic. The simulation results for the thermal load conditions are presented in Tables 7a and b. The results show that the change in airflow rates in the rooms and the atrium is less than 0.05 m^3/s which in not as significant as the change in airflow rates caused by outdoor climate conditions discussed earlier. The comparative results shown in Tables 7 reveal that in the critical case, namely a high outdoor temperature and high internal load, extra ventilation strategies are needed
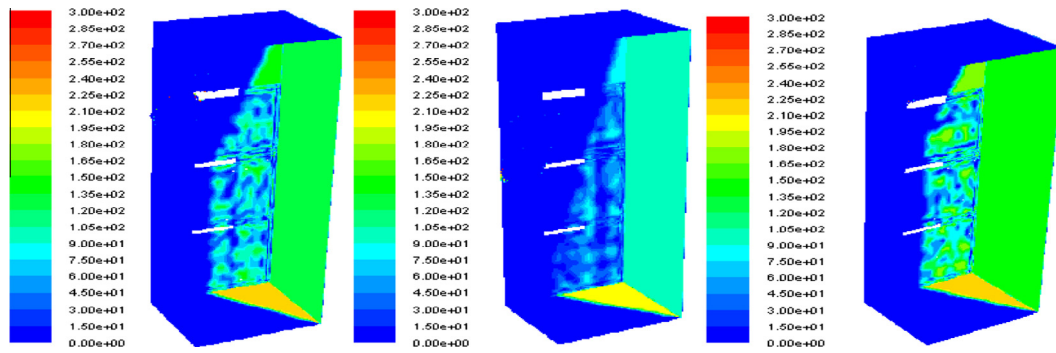
Fig. 11c. Contours of solar heat flux (W/m²) on the façade, east wall and floor of the atrium at 16:00 h in Montreal (Longitude: −73, Latitude: 45) on April, July and September 15, 2010 respectively.
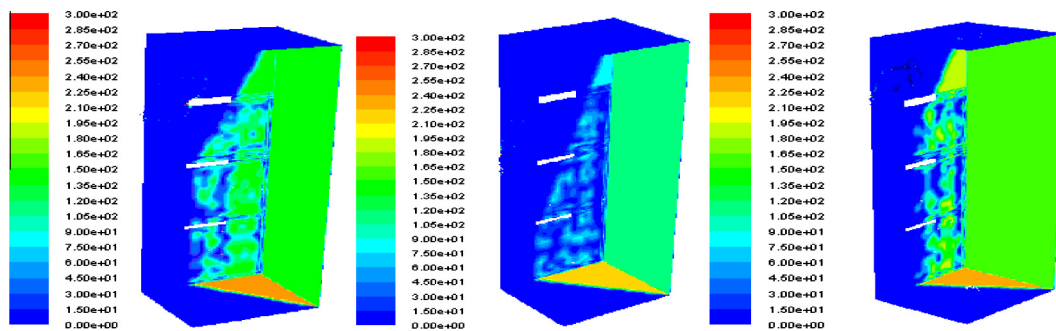
Fig. 11d. Contours of solar heat flux (W/m²) on the façade, east wall and floor of the atrium at 16:00 h in St. John's (Longitude: −52, Latitude: 47) on April, July and September 15, 2010 respectively.

for the building occupied space to reach the required comfort level. Fig. 9a–d shows the contours of pressure, velocity, turbulence intensity, and temperature distributions in the middle plane parallel to the façade surface along the height of the building respectively with each heat source of 200 W/m² at each occupied area of the rooms and atrium floor at 13:00 h on July 15th, 2010. Fig. 9a shows the stack pressure developed which is the pressure difference between the interior and exterior of the building created naturally by density differences caused by warm air generated inside the building due to solar heat gain and heat sources present in the building. This pressure difference drives ventilation flow through the building by means of thermal stack effects. Fig. 9b shows velocity contours of buoyancy-driven ventilation airflow and indicates the influence of gravitational body forces on the velocity fields within the rooms and the atrium space. It was seen that in the presence of solar radiation, free convection effects are shown by the formation of air stream moving upward around the hot surfaces. Strong stack effect creates higher inflow on the lower floors than the upper floors. Fig. 9c presents turbulence intensity contours in the middle plane parallel to the façade surface along the height of the building. The instantaneous velocity vector (u) can be decomposed into mean and turbulent components in the X, Y and Z directions:

$$u_i = U_i + u_i' \tag{13}$$

where U_i is the mean velocities and u_t' is their turbulent counterparts, with index i representing X, Y and Z. The r.m.s of each velocity component, $u_i^{r.m.s}$ is defined as the standard deviation of u_i and the normalized r.m.s. velocity or turbulence intensity is defined as $I_i = u_i^{r.m.s}/U_i$. The results show that turbulence intensity values are nearly uniform along the vents with a tendency of higher values near the outflow than the inflow and in the regions where there is more mixing and circulation of the airflow within the building. Fig. 9d shows temperature distribution within the building. Higher air temperature stratification was observed near the ceilings of the rooms and near the outlet in the atrium walls. Lower temperature stratification near the floors was due to the strong convection. Based on all the contour plots, the authors have carried out a detailed thermal comfort analysis of occupants in terms of velocity, turbulence intensity, temperature and thermal stratification in other papers i.e., see (Hussain and Oosthuizen, 2012b) and (Hussain and Oosthuizen, 2013).

4.5. Effect of Solar Intensity on buoyancy-driven airflows

To determine the ability of the CFD model to predict the effect of solar intensity on the buoyancy-driven air
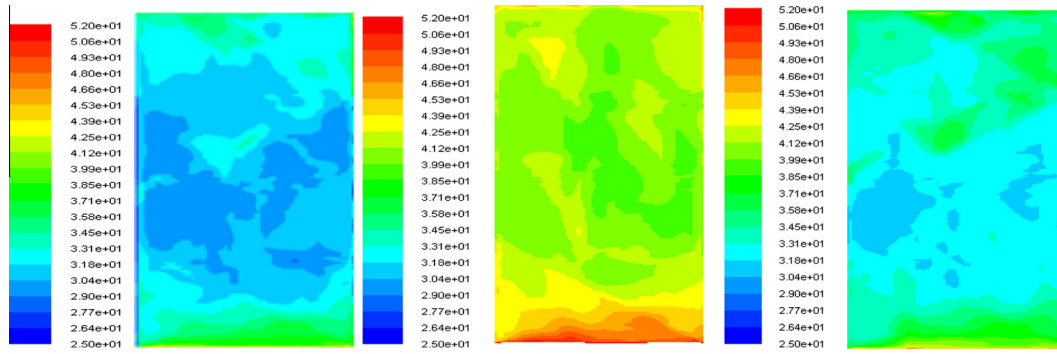
Fig. 12a. Temperature (°C) contours on the façade glazing surface at 13:00 h in Calgary on April, July and September 15, 2010 respectively.
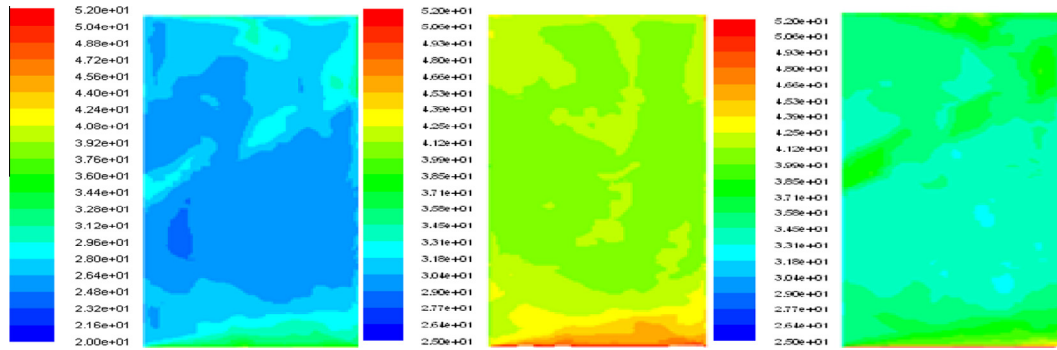
Fig. 12b. Temperature (°C) contours on the façade glazing surface at 13:00 h in Winnipeg on April, July and September 15, 2010 respectively.
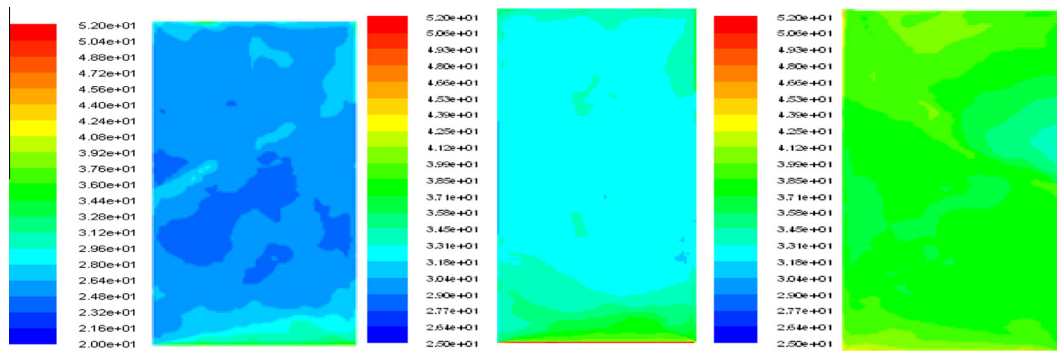
Fig. 12c. Temperature (°C) contours on the façade glazing surface at 13:00 h in Montreal on April, July and September 15, 2010 respectively.

flow at different times of the day, simulations were run at hourly intervals between 6:00 and 18:00 h. The outside boundary conditions such as outside air temperature and the positioning of the sun were adjusted for each particular time using FLUENT© solar calculator. Fig. 10 shows the CFD predictions for the effect of solar intensity on the volume flow rate (m³/s) on an hourly basis in each storey from 6:00 to 18:00 h. It can be seen that with increasing of solar intensity, the volume flow rate increases in the period 6:00–11:00 h and then decreases in the period 11:00–18:00 h with the decrease in solar intensity. The effect of solar intensity also, of course, depends on the direction and location of glazing surfaces of the building.

4.6. The effect of the geographical locations on the buoyancy-driven airflows

In order to investigate the effect of the geographical location on the buoyancy-driven ventilation flow rates the building was assumed to be located with the same orientation in different cities of Canada. Due to the different global location of each city, variation in the solar loading was noticed in each case. The global position and the ambient temperature of each location at 13:00 h on different dates are shown in Table 8. The contours of solar heat flux (W/m²) on the glazed façade, east wall and floor of the atrium were determined through CFD simulations at 13:00 on April, July and September 2010 in different cities and are shown in Figs. 11.
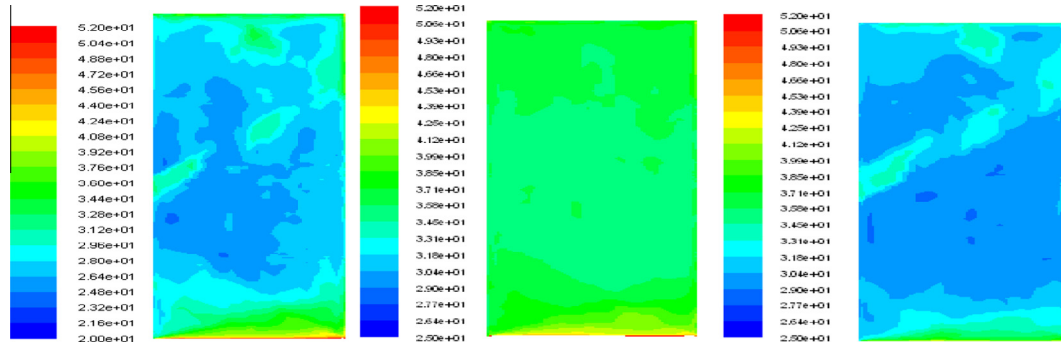
Fig. 12d. Temperature (°C) contours on the façade glazing surface at 13:00 h in St. John's April, July and September 15, 2010 respectively.
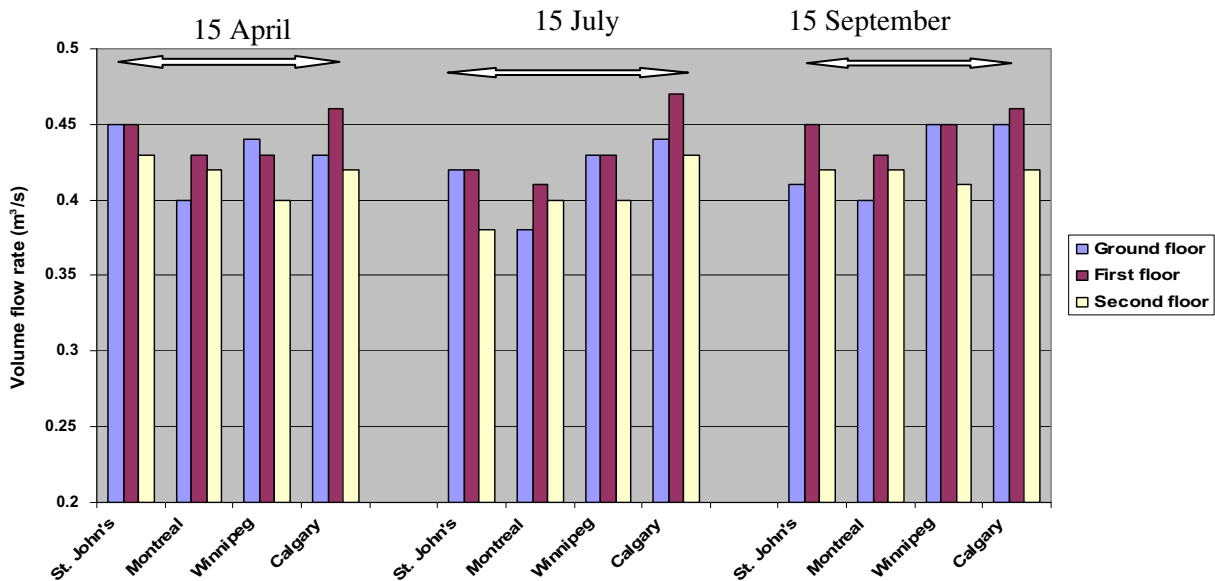
Fig. 13. Effect of geographical location of the building on the volume flow rate with the same ventilation rate in each storey at 13:00 h on April, July and September 15, 2010 in St. John's, Montreal, Winnipeg, Calgary and Vancouver.

It can be seen from Figs. 11 that the solar heat flux in the cities considered varies approximately in the range 75–220 W/m². These variations in the solar heat flux directly affect the predicted glazed façade surface temperatures (°C) as seen from the results shown in Figs. 12. These results indicate that the average glazed façade temperatures at 13:00 h on July 15, 2010 in Calgary, Winnipeg, St. John's and Montreal are approximately 43, 41, 37 and 33 °C, respectively. Solar intensity also varies with different climates and geographical location of the building. The combined effect of the solar intensity at different geographical locations of the building and of the assumed internal heat sources on the ventilation air flow rates (m³/s) in each storey at 13:00 h on April, July and September 15, 2010 was determined and the results are shown in Fig. 13. It was noted with the variation of the geographical location, the solar intensity varies. From the results of Fig. 13 it is seen that where the building has higher glazed façade surface temperatures (°C) due to higher solar intensity, a greater solar driven buoyancy effect inside the building and accord-

ingly an increase in the ventilation air flow rate occurs. It is concluded that solar assisted natural ventilation in an atrium building in addition to other factors also depends upon the geographical location and orientation of the building which should be considered in the initial design of an atrium building.

5. Conclusions

In this study, a simple three-storey atrium building was modeled and the use of buoyancy-driven natural ventilation induced by solar radiation and heat sources was investigated using a validated CFD model. Steady-state CFD simulations of the buoyancy-driven natural ventilation airflow and temperature distributions in the building were carried out utilizing the SST k-ω turbulence model and the DTRM radiation model. The CFD predictions of the volume flow rate expressed in the non-dimensional form were compared with the analytical predictions obtained using the design curves developed by Holford and Hunt

(2003). The following main conclusions were drawn from this study.

1. The design curves developed by Holford and Hunt (2003) are useful in establishing the sizes of air inlet and outlet vents to achieve equal ventilation flow rates in each storey of the atrium building.
2. CFD predictions of the volume flow rates expressed in non-dimensional form agree fairly with the general trends depicted by the design curves developed by Holford and Hunt (2003). However, some discrepancies were observed, this is thought to be due to the assumption in the analytical model that the buoyant layer remains homogenous and hydrostatic for all interface heights which was not the case in the CFD simulations as the interface approached the ceiling.
3. The temperature change and volume airflow rate change caused by the internal thermal load is not as significant as that caused by outdoor climate conditions. Simulation results show that the external ambient temperature has a greater influence on the buoyancy-driven airflow rate and on the temperature distribution inside the building. The variation of internal thermal loads has little influence ($\leqslant 1$ °C or 0.05 m^3/s) on the thermal environment of the building.
4. In hot and humid weather, a building would require a significant height in order to induce a sufficient pressure gradient caused by temperature difference for efficient buoyancy-driven ventilation.
5. Solar intensity and geographical location have considerable effect on the buoyancy-driven flow rate and temperature distributions in the building.
6. CFD techniques can be applied to real buildings to predict airflow parameters such as stratification depth, buoyancy of the upper layer and ventilation flow rate provided that the effective opening areas are accurately represented.
7. The results of this study can be considered at the initial design stage of an energy-efficient atrium building in order to obtain a comfortable indoor thermal environment. Based on this study, future research will include wind speed and other climatic factors.
8. Overall, the proposed methodology provides a useful procedure for building designers to quantify the buoyancy-driven natural ventilation at the initial design stage of an energy-efficient atrium building. It should be mentioned that the CFD modeling approach introduced is general and it can be used to analyze the indoor environment of a building by either turbulence modeling or experimental measurements.

Acknowledgement

References

Allocca, C., Chen, Q., Glicksman, L.R., 2003. Design analysis of single-sided natural ventilation. Energy and Buildings 35, 785–795.

Anne, V., Francois, R.C., Gerard, G., 2001. Thermal and ventilation modeling of large highly-glazed spaces. Energy and Buildings 33, 121–132.

Atif, A., Claridge, D., 1995. Atrium buildings, thermal performance and climatic factors. ASHRAE Transactions 101 (1), 454–460.

Cook, M.J., Lomas, K.L., 1998. Buoyancy-driven displacement ventilation flows: evaluation of two eddy viscosity models for prediction. Building Services Engineering Research and Technology 19, 15–21.

Cook, M.J., Ji, Y., Hunt, G.R., 2003. CFD modeling of natural ventilation: combined wind and buoyancy forces. International Journal of Ventilation 1, 169–180.

Guohui, G., 2006. Simulation of buoyancy induced flow in open cavities for natural ventilation. Energy and Buildings 38, 410–420.

Holford, J.M., Hunt, G.R., 2003. Fundamental atrium design for natural ventilation. Building and Environment 38, 409–426.

Hunt, G.R., Kaye, N.G., 2001. Virtual origin correction for lazy turbulent plumes. Journal of Fluid Mechanics 435, 377–396.

Hussain, S., Oosthuizen, P.H., 2010. An evaluation of turbulence models for the numerical study of flow and temperature distribution in atria. In: Proceedings of 18th Annual Conference of the CFD Society of Canada, London Ontario, May 17–19, 2010.

Hussain, S., Oosthuizen, P.H., 2011. Validation of numerical study of flow and temperature distribution in an atrium space. In: Proceedings of 19th Annual Conference of the CFD Society of Canada, Montreal, Canada, April 27–29, 2011.

Hussain, S., Oosthuizen, P.H., 2011. Numerical study of an atrium integrated with hybrid ventilation system. In: Proceedings of 23rd Canadian Congress of Applied Mechanics, Vancouver, BC, Canada, June 5–9, 2011.

Hussain, S., Oosthuizen, P.H., 2012a. Validation of numerical modeling of conditions in an atrium space with a hybrid ventilation system. Building and Environment 52, 152–161.

Hussain, S., Oosthuizen, P.H., 2012b. Numerical investigations of buoyancy-driven natural ventilation in a simple three-storey atrium building and its effect on thermal comfort conditions. Applied Thermal Engineering 40, 358–372.

Hussain, S., Oosthuizen, P.H., 2013. Numerical investigations of buoyancy-driven natural ventilation in a simple three- storey atrium building and thermal comfort evaluation. Applied Thermal Engineering 57, 1–14.

Hussain, S., Oosthuizen, P.H., Kalendar, A., 2011. Evaluation of various turbulence models for the prediction of the airflow and temperature distributions in atria. Energy and Buildings 48, 18–28.

Ji, Y., 2004. Numerical studies on natural ventilation flow in an enclosure with both buoyancy and wind effect. In: CIBSE National Conference: Delivering Sustainable Construction, London, UK, 28–29 September 2004.

Ji, Y., 2007. Numerical studies of displacement natural ventilation in multi-storied buildings connected to an atrium. Building Services Engineering Research and Technology 28 (3), 207–222.

Jiang, Y., Allocca, C., Chen, Q., 2004. Validation of CFD simulations for natural ventilation. International Journal of Ventilation 2 (4), 359–370.

Josef, T., Vitaly, H., Meir, T., 2008. Airflow and heat flux through the vertical opening of buoyancy- induced naturally ventilated enclosures. Energy and Buildings 40, 637–646.

Josef, T., Vitaly, H., Meir, T., 2008. Airflow and heat flux through the vertical opening of buoyancy-induced naturally ventilated enclosures. Energy and Buildings 40, 637–646.

Kevin, J.L., 2007. Architectural design of an advanced naturally ventilated building form. Energy and Buildings 39, 166–181.

Linden, P.F., Serff, G.L., Smeed, D.A., 1990. Emptying filling boxes: the fluid mechanics of natural ventilation. Journal of Fluid Mechanics 212, 309–335.

Mills, A.F., 1999. Heat Transfer, second ed. Prentice Hall, New Jersey, pp. 570–572.

Morton, B.R., Taylor, G.I., Turner, J.S., 1956. Turbulent gravitational convection from maintained and instantaneous sources. In: Proceedings of the Royal Society A; 234, 1–23.

Mouriki E., 2009. Solar-assisted hybrid-ventilation in an institutional building. M.Sc Thesis, Department of Building, Civil and Environmental Engineering, Concordia University, Montreal, Canada.

Oosthuizen, P.H., Lightstone, M., 2009. Numerical analysis of the flow and temperature distributions in an atrium. In: Proceedings of the Conference on Computational Methods for Energy Engineering and Environment-ICCM3E, Sousse, November 20–22, 2009.

Palyvos, J.A., 2008. A survey of wind convection coefficient correlations for building envelope energy systems, modeling. Applied Thermal Engineering 28, 801–810.

Rundle, C.A., Lightstone, M.F., Oosthuizen, P.H., Karava, P., Mouriki, E., 2011. Validation of computational fluid dynamics simulations for atria geometries. Buildings and Environment 46, 1343–1353.

Stamou, A., Katsiris, I., 2006. Verification of a CFD model for indoor airflow and heat transfer. Buildings and Environment 41, 1171–1181.

Stavrakakis, G., Koukou, M., 2008. Natural cross-ventilation in buildings: building-scale experiments, numerical simulation and thermal comfort evaluation. Energy and Buildings 40, 1666–1681.

Tahir, A., Osman, Y., 2005. Investigating the potential use of natural ventilation in new building design. Energy and Buildings 38, 959–963.

Tsou, J.Y., 2001. Strategy on applying computational fluid dynamic for building performance evaluation. Automation in Construction 10, 327–335.

Walsh, P.C., Leong, W.H., 2004. Effectiveness of several turbulence models in natural convection. International Journal of Numerical Methods for Heat and Fluid Flow 14, 633–648.

Xin, W., Chen, H., Weiwu, C., 2009. Mathematical modeling and experimental study on vertical temperature distribution of hybrid ventilation in an atrium building. Energy and Buildings 41, 907–914.

Zhai, Z., 2006. Application of computational fluid dynamics in building design: aspects and trends. Indoor and Built Environment 15 (4), 305–313.